Dynamics of Interfacial Electron Transfer from Photoexcited Quinizarin (Qz) into the Conduction Band of TiO_2 and Surface States of ZrO_2 Nanoparticles

G. Ramakrishna, Ajay K. Singh, Dipak K. Palit, and Hirendra N. Ghosh*

Radiation Chemistry & Chemical Dynamics Division, Bhabha Atomic Research Center, Trombay, Mumbai 400 085, India

Received: September 3, 2003; In Final Form: February 4, 2004

Electron injection and back-electron-transfer (BET) dynamics of quinizarin (Qz) adsorbed on TiO_2 and ZrO_2 nanoparticles has been studied by femtosecond transient absorption spectroscopy in the visible and near-IR region. A good fraction of Qz forms a charge-transfer (CT) complex while being adsorbed on the TiO_2 or ZrO_2 nanoparticles surface. Following photoexcitation of Qz/TiO_2 and Qz/ZrO_2 systems, electron injection into the nanoparticles has been confirmed for both the systems by direct detection of electron in the nanoparticle and cation radical of Qz ($Qz^{\cdot+}$). The dynamics of BET from TiO_2 and ZrO_2 to the parent cation has been measured by monitoring the decay kinetics of $Qz^{\bullet+}$ and electron in the nanoparticles and it is found to be multiexponential. As S_1 state of Qz lies below the conduction band edge of ZrO_2 so electron injection from S_1 state into the nanoparticle is not thermodynamically possible. However, the detection of $Qz^{\bullet+}$ as well as injected electrons in the case of Qz/ZrO_2 system confirms that electron injection also takes place in ZrO_2. We have attributed this to the injection into surface states of ZrO_2 nanoparticles. It has been observed that electron injection takes place in <50 fs and the majority of the injected electrons come back to the parent cation with a time constant of <1 ps for both the systems. We have observed multiphasic recombination dynamics with time constants ranging from $\sim$600 fs to the pico-, nano-, and microsecond time scale for both Qz/TiO_2 and Qz/ZrO_2 systems. Our investigation has revealed that electron injection into the surface states of nanoparticles is possible or facilitated when the adsorbed sensitizer molecule forms a strong CT complex with the semiconductor nanoparticles.

1. Introduction

Dye sensitization of wide band gap semiconductor electrodes has gained sufficient attention in recent years, largely due to the demonstration of dye-sensitized solar cells with conversion efficiency as high as 10%.[1,2] The mechanism of solar cell devices is based upon the injection of an electron from a photoexcited state of the sensitized dye into the conduction band of the semiconductor. The efficiency of the dye-sensitized solar cells depends critically on the rates of the forward (dye to semiconductor) and back (semiconductor to dye) electron-transfer (BET) reactions. For an efficient solar energy conversion it is necessary to establish conditions for both fast electron injection and slow recombination. The high yield of long-lived charge separation is expected for useful conversion of sunlight into electric charge. However, the detailed mechanisms, the nature, and the rate of electron injection into the semiconductor and factors determining the rate of BET are not well understood.

The basic photophysical process in a solar cell device is the electron injection from the electronically excited state of the adsorbed dye into the conduction band of the nanoparticle, which takes place in fast and ultrafast time scale.[3−30] The resulting charge-separated system has been reported to undergo relaxation and recombination in different adsorbate dye−nanoparticle systems ranging from picoseconds,[3−10,17−30] nanoseconds,[3,11−14] up to microseconds,[15,16] and even milliseconds.[15,16] Theoretical studies have indicated that BET dynamics in dye-sensitized nanoparticles is often controlled by trapping and detrapping dynamics of the injected electrons.[31,32] Marcus theory predicts that the rate of electron transfer (electron injection or BET) depends on the free energy (ΔG) between the donor and acceptor states. Thus energetic position of the donor and acceptor levels plays a key role for the dynamics of electron injection and BET reactions. So far as the electron injection is concerned, reports are available only for injection to the conduction band (high density of states) of the nanoparticle except the one reported by Huber et al.[30] and the other one reported very recently by Olsen et al.[33] Huber et al.[30] have reported ultrafast electron injection into the surface states of ZrO_2 nanoparticles sensitized by alizarin. Olsen et al.[33] have reported electron injection dynamics of Ru^{II}(4,4′-dicarboxy-2,2′-bipyridine)$_2$(SCN)$_2$ (the so-called N3-dye) adsorbed on colloidal ZrO_2 nanoparticles in solution at room temperature using time-resolved absorption polarization spectroscopy. Recently, Hao et al.[34] have demonstrated electron injection into the surface states of ZrO_2 nanoparticles with different crystallinities. It is very difficult to investigate the electron injection into the surface states of relatively lower band gap nanoparticles such as TiO_2 where the injection process takes place immediately in the lower lying high-density conduction band. Because the band gap for the ZrO_2 nanoparticle is very high, it is an ideal system to study electron injection into the surface states of nanoparticle and BET reactions. To see the electron injection into the surface states of the ZrO_2 nanoparticle, it is important to have strong coupling between the adsorbed dye molecule and the nanoparticles.

In the present investigation we have reported the electron injection and BET dynamics of Qz adsorbed onto the TiO_2 and

* Corresponding author. E-mail: hnghosh@magnum.barc.ernet.in.

10.1021/jp036623r CCC: $27.50
Published on Web 03/19/2004

ZrO_2 nanoparticles. The quinoid moiety of Qz forms a CT complex with ZrO_2 nanoparticles. Electron injection into TiO_2 and ZrO_2 nanoparticles has been confirmed by monitoring the cation radical and injected electron in the nanoparticles using transient absorption measurements in the femtosecond time domain. The observation of the cation radical spectrum in the case of ZrO_2 suggests that electron injection takes place in ZrO_2. We have attributed this to the injection into the surface states of ZrO_2 nanoparticles. Electron injection time measured to be <50 fs and recombination kinetics can be fitted multiexponentially, where the majority of the injected electrons come back to the parent cation radical with a time constant of ~600 fs for both the systems. Ultrafast recombination dynamics of injected electrons and parent cation radicals indicate strong coupling matrix for BET process of the above system. In the present investigation we have observed that electron injection into the surface states of ZrO_2 nanoparticles is facilitated by the formation of a CT complex of the dye with nanoparticles.

2. Experimental Section

(a) Materials. Quinizarin (Qz) was obtained from Fluka and was purified by crystallization. Titanium(IV) tetraisopropoxide $\{Ti[OCH(CH_3)_2]_4\}$ (Aldrich, 97%), methanol (Aldrich) and isopropyl alcohol (Aldrich) were purified by distillation. Zirconium(IV) isopropoxide 2-propanol complex $Zr[OCH(CH_3)_2]_4 \cdot (CH_3)_2CHOH$ (Aldrich, 99.9%) was used without further purification. Nanopure water (Barnsted System) was used for making aqueous solutions.

(b) Sample Preparation. Nanometer-size TiO_2 was prepared by controlled hydrolysis of titanium(IV) tetraisopropoxide.[3,35−37] A solution of 5 mL of $Ti[OCH(CH_3)_2]_4$ (Aldrich, 97%) dissolved in 95 mL of isopropyl alcohol (Aldrich) was added dropwise (1 mL/min) to 900 mL of Nanopure water (2 °C) at pH 1.5 (adjusted with HNO_3). The solution was continuously stirred for 10−12 h until a transparent colloid was formed. The colloidal solution was concentrated at 35−40 °C with a rotary evaporator and then dried with a nitrogen stream to yield a white powder. The ZrO_2 nanoparticle was also prepared by adopting the above procedure. X-ray diffraction measurements indicated that the crystal structure of TiO_2 is anatase.[34] However, ZrO_2 nanoparticles are cubic.[38] The hydrodynamic diameter of both TiO_2[37] and ZrO_2[39] colloidal particles was found to be 5−6 nm, as determined by dynamic light scattering measurements. We have carried out sensitization of nanoparticles by adding solid Qz to the aqueous colloids under continuous stirring conditions. As Qz is not soluble in water, the solvation process supports the coupling of Qz with both semiconductors. Through other procedures we have sensitized the nanoparticles, by presolving Qz in methanol and then adding the dissolved dye into the aqueous colloidal solution (net volume fraction <5% methanol). The resulting solution is kept for half an hour in stirring conditions to form a complex of the dye with the nanoparticle. The optical absorption spectra of the dye-sensitized nanoparticles, as prepared by adopting the above two procedures, look very similar. The concentration of the dye is about 200 μM for transient absorption measurements and it is 12 μM for ground-state absorption and fluorescence measurements. Typical concentrations of the nanoparticles for the transient experiments (both TiO_2 and ZrO_2) were kept at 40 gm/L. For the entire measurements sample solutions were deoxygenated by continuously bubbling high-purity nitrogen (99.95 Iolar grade from Indian Oxygen Co. Ltd., India) through the solutions. The solutions are flowed through a 2 mm path quartz cell during all the measurements. Experimental samples were quite stable, as we have observed that the absorption spectra of the dye−nanoparticle system before and after laser experiments were identical.

(c) Femtosecond Visible Spectrometer. The femtosecond tunable visible spectrometer has been developed on the basis of a multipass amplified femtosecond Ti:sapphire laser system from Avesta, Russia (1 kHz repetition rate at 800 nm, 50 fs, 800 μJ/pulse), and described earlier.[40] The 800 nm output pulse from the multipass amplifier is split into two parts to generate pump and probe pulses. One part, with 200 μJ/pulse, is frequency doubled in BBO crystals to generate pump pulses at 400. To generate visible probe pulses, about 3 μJ of the 800 nm beam is focused onto a 1.5 mm thick sapphire window. The intensity of the 800 nm beam is adjusted by iris size and ND filters to obtain a stable white light continuum in the 400 to over 1000 nm region. The probe pulses are split into the signal and reference beams and are detected by two matched photodiodes with variable gain. We have kept the spot sizes of the pump beam and probe beam at the crossing point around 500 and 300 μm, respectively. The excitation energy density (at 400 nm) was adjusted to ~2500 μJ/cm^2. The noise level of the white light is about ~0.5% with occasional spikes due to oscillator fluctuation. We have noticed that most laser noise is low-frequency noise and can be eliminated by comparing the adjacent probe laser pulses (pump blocked vs unblocked using a mechanical chopper). The typical noise in the measured absorbance change is about <0.3%. The instrument response function was obtained by fitting the rise time of the bleach of sodium salt of *meso*-tetrakis(4-sulfonatophenyl)porphyrin (TPPS) (at ~pH 1) at 710 nm, which has an instantaneous response.

(d) Cyclic Voltammetry. Voltammetric experiments were performed with Auto Lab PGSTAT 20 (Manufactured by Eco-Chemie, Netharlands) coupled to a Metrohm 663 VA stand electrode system comprising a glassy carbon (GC)/Pt/Ag/AgCl. The PG STAT was driven by Autolab software. The temperature of the solution was maintained at 25 ± 0.1 °C. Measurements were done in acetonitrile solution with TEAP (triethylammonium perchlorate) as a supporting electrolyte and in N_2 atmosphere. The oxidation redox potential of the Qz molecule has been determined to be 1.63 V against the Ag/AgCl electrode.

3. Results and Discussion

(a) Dye Binding and Formation of Charge-Transfer (CT) Complex. To understand the mechanism of the dye-sensitized ET reaction in the dye−nanoparticles system, it is very important to know the type of interaction between the dye molecules and the nanoparticles when they get adsorbed on the nanoparticle surface. We have carried out steady-state absorption measurements of Qz molecules in TiO_2 and ZrO_2 colloidal solutions. Figure 1 shows the absorption of free Qz in water and Qz adsorbed on ZrO_2 nanoparticles. The optical absorption spectrum of Qz in water at 2.5 pH shows a peak at 485 nm with a shoulder at 542 nm. On addition of ZrO_2 nanoparticles, the absorption spectrum of Qz is red shifted with an increase of absorbance. The color of the solution changes from violet to dark pink on addition of ZrO_2. The effect of increasing ZrO_2 concentration on the absorption spectrum is also shown in Figure 1. Quinizarin shows a peak at 525 nm with a shoulder at 562 nm as it is adsorbed on ZrO_2 nanoparticles (at the highest particle concentration). The increment of optical density and the appearance of the red-shifted absorption band indicate a strong electronic coupling between Qz and ZrO_2 nanoparticle and a CT type of interaction. Formation of the CT complex of dye molecules on the TiO_2 particles surface has already been reported in our earlier

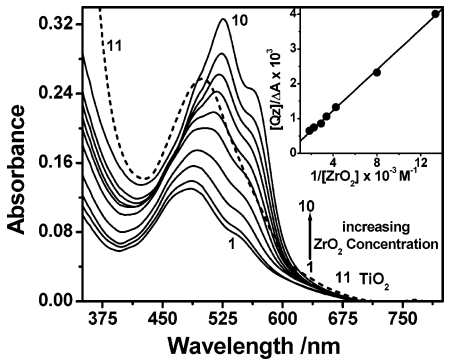

Figure 1. Absorption spectra of quinizarin dye in the presence of various ZrO_2 concentrations. Conditions: 12 μM Qz dye in 1 cm optical path length. ZrO_2 concentrations are (1) 0.0, (2) 0.5, (3) 1.5, (4) 3.5, (5) 4.7, (6) 5.9, (7) 6.9, (8) 8.9, (9) 10.9, and (10) 20 g L^{-1}. (11) Qz dye on TiO_2 (20 g L^{-1}) nanoparticles. pH of all the above solutions is 2.5. (Inset: Benesi−Hildebrandt plot of the Qz/ZrO_2 complex monitored at 560 nm.)

CHART 1: Molecular Structure of the Quinizarin Coupled with ZrO_2

studies.[4,5] The effect of pH on the nanoparticle surface may change the optical absorption spectrum of Qz because surface pH is lower than bulk pH. In the present investigation we have kept the pH of all the above solutions at 2.5. It has already been reported[41] that pK_a for the Qz molecule is 9.9. It has been observed that in a lower pH range (1−9), the optical absorption spectrum of Qz molecule[41] remains unchanged, even if the pH of the nanoparticles surface is little different from the bulk, which will not affect deprotonation from the OH group. We have kept the concentration of Qz molecules at around 12 μM for our optical absorption experiments on the nanoparticle surface. At this low concentration, the probability of aggregation is insignificant.

The results obtained from the above optical absorption studies indicate that on adsorption of the dye molecule on the ZrO_2 nanoparticle surface, a new ligand to metal CT band is formed. It is reported in the literature[41] that Qz molecules form intramolecular H-bonding in water. In the presence of ZrO_2 or TiO_2 nanoparticles, intramolecular H-bonding in the Qz molecule breaks and it forms a six-membered chelate type complex with the nanoparticle (Chart 1). Formation of a CT complex between the TiO_2 nanoparticle and the organic dyes[3,4,42,43] as well as inorganic molecules[18,22,25] is a well-known phenomenon. It has been shown by Huber et al.[30] that the red shift in the absorption maxima and increase in the molar extinction coefficient of the dye due to adsorption on TiO_2 nanoparticle surface is supported by MO calculations for a LMCT type of π−d transition. In the present investigation, we have also observed that Qz forms a complex with ZrO_2 nanoparticles in the ground state. The formation of CT complex can be explained by the following equation

$$ZrO_2 + Qz \rightarrow [ZrO_2^{\delta-} \cdots Qz^{\delta+}]_{Complex} \qquad (1)$$

SCHEME 1: Mechanistic Scheme of Electron Transfer for the Coupled Systems Quinizarin/TiO_2 (Left) and Quinizarin/ZrO_2 (Right)[a]

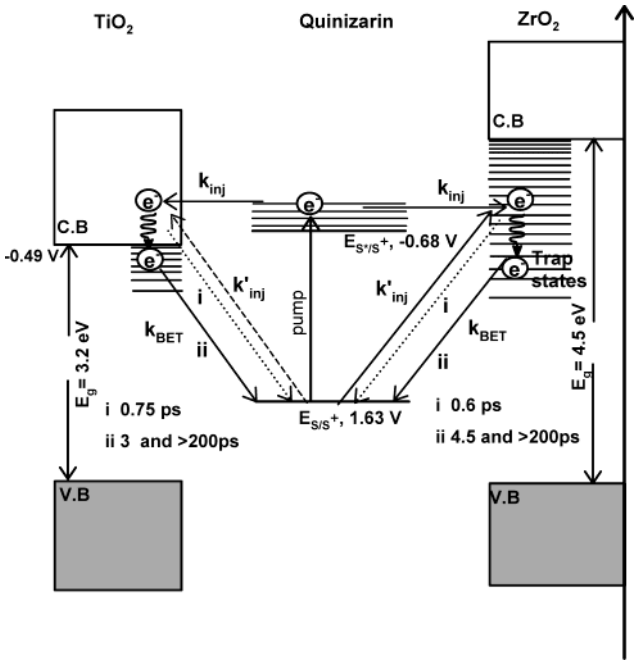

[a] Here S^*/S^+ is the excited sensitized dye/cation radical couple, k_{BET} is the back-electron-transfer rate, k_{inj} is the electron injection through the excited state, k'_{inj} is direct electron injection (excitation of CT complex).

The experimental observation can be explained in the following manner. When Qz molecules are adsorbed on the surface, a fraction of the dye molecules just get adsorbed on the surface of the nanoparticle and a good fraction of the molecules form a CT complex. The modified Benesi−Hilderbandt equation[44] has been used to explain the charge-transfer nature of the dye−nanoparticles system. For the CT interaction, it can be represented as

$$Qz^- + {=}M{-}OH_2^+ \xrightarrow{K_{eq}} {=}M{-}Qz + H_2O \qquad (2)$$

Because the particle concentration is proportional to the concentration of surface hydroxyl groups (${=}M{-}OH_2^+$), we can define the equilibrium constant as

$$K_{eq} = \frac{[M{-}Qz]}{[Qz][MO_2]} \qquad (3)$$

where [Qz] is the concentration of the adsorbed dye, which does not form, complex, [MO_2] is the particle concentration, and [M−Qz] is the concentration of the complex. Eventually from the Benesi−Hilderbandt plot we have determined the molar extinction coefficient of the ZrO_2−Qz complex and it is found to be 15 486 cm^{-1} mol^{-1}. Although Benesi−Hilderbandt analysis is used for molecular complexes and Langmuir isotherm is used for bulk catalysis, for small particles both approaches can be used to define the complex nature of the dye-nanoparticles system. To determine the percentage of dye molecules on the nanoparticle surface, we have used a Langmuir-type adsorption isotherm.[8,38] We have determined the association constants (at equilibrium condition) for both the Qz/ZrO_2 system and the Qz/TiO_2 system with varying dye concentrations following the Langmuir-type adsorption isotherm.[42] Association constants are determined to be 9000 ± 1500 and 6400 ± 800

M^{-1} for the Qz/ZrO_2 and Q/TiO_2 systems, respectively. These results indicate that Qz has a stronger chemical interaction with ZrO_2 nanoparticles compared to that with TiO_2 nanoparticles. The percentage of Qz molecules adsorbed are determined to be >95% on the ZrO_2 surface and >93% on the TiO_2 surface at 0.2 mM Qz concentration and 2 mM nanoparticle (both TiO_2 and ZrO_2) concentration.

Figure 1 shows that on addition of ZrO_2 nanoparticles to an aqueous solution of Qz, the optical absorption spectrum becomes broad and shifts to longer wavelength and the optical density increases. It is interesting to observe from Figure 1 that optical absorption spectra of the Qz molecule in the presence of ZrO_2 nanoparticles are broader and red shifted as compared to that in the presence of TiO_2 nanoparticles. It has already been reported by Rajh et al.[38] that six-membered ring complexes are more stable on the ZrO_2 nanoparticle surface, and five-membered ring complexes are more stable on the TiO_2 nanoparticle surface for <20 nm particles. In the present investigation Qz forms a chelating type of complex having a six-membered ring with ZrO_2 nanoparticles (Chart 1) forming a stronger complex, as compared to that formed on the TiO_2 nanoparticle surface. In this chart, it can be seen that oxygen bonded to the central ring in keto (quinoid) form along with one OH group binds to the Zr(IV) atom, which is sitting on the surface of the nanoparticle. This binding mode results in a six-membered ring chelate type of complex with the surface Zr atoms. A six-membered ring has larger bond angles that can accommodate the cubic structure of ZrO_2. On the other hand, Chen et al.[45,46] as well as we[5] have observed that the TiO_2 nanoparticle with smaller particle sizes (size <20 nm) forms a stable five-membered ring chelate type of strong CT complex as compared to that of the six-membered one, with adsorbed dye molecules. In the present studies, because Qz can form only a six-membered ring with TiO_2 nanoparticles and hence it forms a relatively weaker CT complex with TiO_2 as compared to that with ZrO_2 nanoparticles.

To study electron-transfer reaction for strongly coupled dyes with nanoparticles, it is very important to know about electronic coupling element H_{ab}. If H_{ab} is not too small, it can be calculated from spectroscopies quantities. The expression generally used for this purpose is given by eq 4 from Mulliken[47] and Hush,[48] where the band maximum $\bar{\nu}_{max}$ and bandwidth $\Delta\bar{\nu}_{1/2}$ are in reciprocal centimeters, the molar absorptivity ϵ_{max} has units of reciprocal mole centimeters, and the donor−acceptor separation r_{ab} is in angstroms:

$$H_{ab} = \frac{2.06 \times 10^{-2}(\bar{\nu}_{max}\epsilon_{max}\Delta\bar{\nu}_{1/2})^{1/2}}{r_{ab}} \qquad (4)$$

For an ET reaction, it is evident that H_{ab} is a very important parameter. In the present investigation we have determined H_{ab} for the Qz/ZrO_2 system using the Mulliken and Hush equation[47,48] and found it to be 5561 cm^{-1}. The value of H_{ab} in the Qz/ZrO_2 system is quite high and comparable to strongly coupled triphenylmethane dyes with TiO_2 nanoparticles.[5]

(b) Excited-State Dynamics of Free Quinizarin. We have carried out transient absorption measurements to study excited-state dynamics of the Qz molecule in methanol exciting with 400 nm laser light. The solubility of the Qz molecule in water is very poor, so to study the excited-state dynamics of free Qz, we have chosen methanol as a solvent. Figure 2 shows transient absorption spectra at different time delays, which consist of absorption peaks at 530 and 830 nm and a negative absorption band with a peak at 610 nm with a shoulder at 660 nm. The transient absorption peaks at 530 and 830 nm have been attributed to the excited singlet state absorption (ESA) and the negative absorption band has been attributed to the stimulated emission. The inset in Figure 2 shows the kinetic decay trace of the stimulated emission at 610 nm (reversed) and excited singlet state at 830 nm. Both the dynamics matched very well, and excited-state decay fitted with a lifetime greater than 1 ns. Time-resolved fluorescence measurements on Qz in methanol and water (dissolved in 5% methanol + 95% water) have also been carried out using time-correlated single photon counting. Single-exponential lifetimes of 1.86 ns ($\chi^2 = 0.98$) and 1.47 ns ($\chi^2 = 1.09$) are observed in methanol and water, respectively.

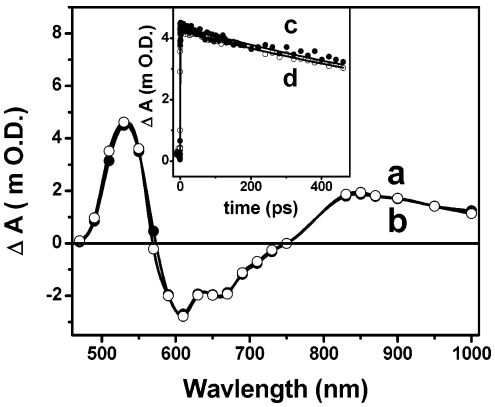

Figure 2. Transient absorption spectra of quinizarin in methanol at (a) 1 ps and (b) 10 ps delay time. The transient absorption peaks at 530 and 830 nm have been attributed to the excited singlet state, and the negative absorption band peaking at 610 nm has been attributed to stimulated emission. Inset: transient absorption decay at 830 nm (c), and stimulated emission decay (reversed) (d). Typical concentration of the Qz was kept ~200 μM.

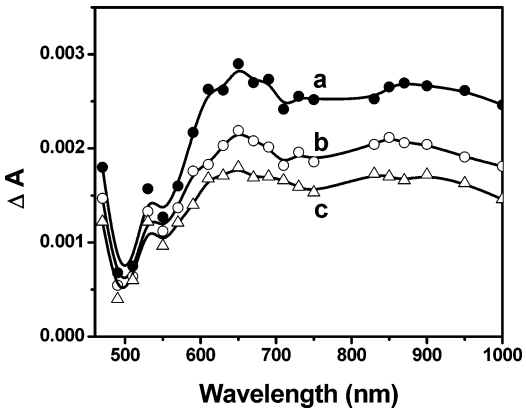

Figure 3. Transient absorption spectra of quinizarin-sensitized TiO_2 nanoparticle in water at (a) 100 fs, (b) 500 fs, and (c) 1 ps after excitation at 400 nm. The spectrum at each time delay consists of an absorption peak at 650 nm and a broad positive absorption feature in the whole spectral region (700−1000 nm). These features are assigned to cation radical of Qz dye and injected electron in nanoparticles, respectively. The typical concentration of the Qz molecules was ~200 μM and of TiO_2 particles was ~40 g/L.

(c) Transient Absorption Measurements in the Quinizarin/TiO_2 System. It has been demonstrated by many workers that optically excited dye molecules adsorbed on the TiO_2 nanoparticle surface injects electrons into the conduction band of the nanoparticle.[3−30] In the present investigation, we have carried out femtosecond laser flash photolysis experiments exciting the Qz/TiO_2 system with 400 nm laser light to study the ET dynamics on semiconductor surface. Figure 3 shows the time-resolved transient absorption spectra of Qz-sensitized TiO_2 nanoparticles in water. The spectrum at each time delay consists

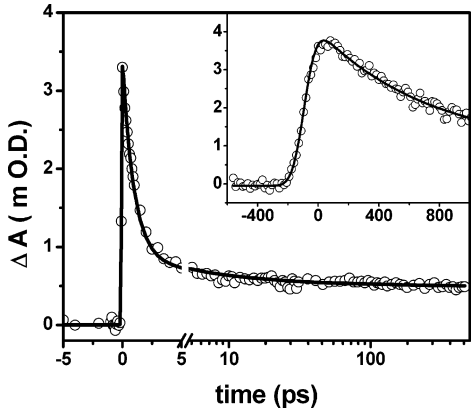

Figure 4. Decay kinetics of the injected electron at 900 nm in Qz/TiO_2 system exciting with 400 nm laser pulse. The solid lines are best fits to the data. The inset shows the same kinetics in a shorter time scale, demonstrating electron injection time (<50 fs).

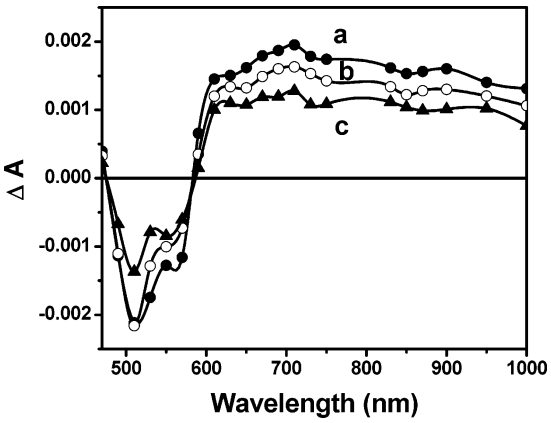

Figure 5. Transient absorption spectra of quinizarin-sensitized ZrO_2 nanoparticle in water at (a) 100 fs, (b) 500 fs, and (c) 1 ps after excitation at 400 nm. The spectrum at each time delay consists of a bleach in the 470−580 nm region centered at 520 nm with a shoulder at 560 nm, an absorption peak at 650 nm, and a broad positive absorption feature in the whole spectral region (700−1000 nm). These features are assigned to the ground-state bleach of the Qz dye, the cation radical of the Qz dye, and the injected electron in the nanoparticles, respectively. The typical concentration of the Qz molecules was ~200 μM and of the ZrO_2 particles was ~40 gm/L.

of an absorption band with a peak at 650 nm and also a broad absorption band from 700 to 1000 nm. The broad spectral absorption in 700−1000 nm region is attributed to the conduction band electrons in the nanoparticles (e_{CB}^-). It has already been shown by many workers that the conduction band electrons can be detected both by visible[29,30,49−51] and by infrared absorption.[23−28] We have measured the electron injection time in the nanoparticles by monitoring the appearance signal of $Qz^{\bullet+}$ at 650 nm as well as e_{CB}^- at 900 nm and found it to be <50 fs (inset, Figure 4). The band having a maximum at 650 nm is assigned to the Qz cation radical ($Qz^{\bullet+}$). Assignment of this band has been made on the basis of the results obtained in separate pulse radiolysis experiments,[52] where $Qz^{\bullet+}$ was generated selectively by the one-electron oxidation reaction of Qz in N_2-bubbled CCl_4 solution. The transient spectrum obtained from pulse radiolysis experiment shows an absorption peak at 450 nm with a broad shoulder at 650 nm. To ensure that the observed transient absorption spectra are due to the photoexcitation of Qz-sensitized TiO_2 colloid, experiments with unsensitized TiO_2/water were performed. No transient signals have been observed following 400 nm excitation. It should be noted that the ground-state UV/vis spectrum of the TiO_2 colloid shows no absorption at 400 nm. The above sensitization process can be presented by the following equation.

$$TiO_2 + Qz \leftrightarrow [TiO_2{-}Qz]_{Adsorb} \xrightarrow[\text{electron injection}]{h\nu} e^-_{cb}(TiO_2) + Qz^+ \quad (5)$$

However, in the transient spectra (Figure 3), we have observed that the transient signal in the 650 nm region and also in the near-IR region decay rapidly with time. This decay of the signals has been attributed to charge recombination or BET from he nanoparticles to the parent cation, which can be expressed in the equation below.

$$e^-_{cb}(TiO_2) + Qz^{\bullet+} \xrightarrow{\text{recombination}} [TiO_2{-}Qz]_{Adsorb} \quad (6)$$

Recombination dynamics of the above reaction has been determined by both monitoring the $Qz^{\bullet+}$ at 650 nm and also the electron in the conduction band at 900 nm. Figure 4 shows the kinetic decay trace for the conduction band electron at 900 nm. We have observed that the BET reaction for Qz/TiO_2 is very fast. Recombination reaction has been found to be multiexponential function with the time constants of 0.75 ps (59.7%), 3 ps (24.4%), and >200 ps (15.9%) (Table 1). We

TABLE 1: Parameters for the Multiexponential Fits to the BET Kinetics of Sensitized TiO_2 and ZrO_2 Nanoparticles

system	$1/k_1$ (A_1)	$1/k_2$ (A_2)	$1/k_3$ (A_3)
Qz-TiO_2	0.75 ps (59.7%),	3 ps (24.4%)	>200 ps (15.9%)
Qz-ZrO_2	0.6 ps (76.2%),	4.5ps (10.8%)	>200 ps (13%)

have also monitored the decay of the cation radical at 650 nm, where the kinetic decay trace of the cation has been fitted multiexponentially with similar time constants as that of the recombination of e_{CB}^- at 900 nm. However, the transient absorption at 650 nm is both due to transient absorption of the Qz cation radical as well as the conduction band electron. So, for the recombination reaction we have preferred to monitor the decay kinetics at 900 nm, where only the electron in the nanoparticles absorbs. The long-time offset (which persists to a delay time of τ > 460 ps) of the transients for the Qz/TiO_2 system (Figure 4) can be assigned to the slow recombination reaction of the long-lived charge-separated state. This process continues to occur in nanosecond to microsecond time scale.[52] Slow recombination reaction is due to those electrons, which move to different trap sites with a distribution of trap energy and distance from the adsorbate. As a result, the recombination reaction is multiexponential with many slower components.

(d) Transient Absorption Measurements in the Quinizarin/ZrO_2 System. Considering that the surface nature of ZrO_2 nanoparticles is very similar to that of the TiO_2 nanoparticle,[53] in our previous investigations[3,4] on the dye-sensitized TiO_2 nanoparticle reaction to understand the photophysics of the dye molecule on a noninjecting nanoparticle surface, we have used ZrO_2 nanoparticles. As the conduction band edge of ZrO_2 nanoparticles is 1.3 eV higher than that of TiO_2 nanoparticles, electron injection is not possible from the photoexcited dye molecules. So in those studies,[3,4] we observed that excited-state properties of the dye molecules on ZrO_2 nanoparticles surface are very similar to that in bulk solvents. In the present investigation we have carried out femtosecond laser spectroscopic experiments on Qz molecules adsorbed on the ZrO_2 nanoparticle exciting at 400 nm, to study the excited-state dynamics on a noninjecting semiconductor surface. Figure 5 shows the time-resolved transient absorption spectra of the Qz/ZrO_2 system in water. The spectrum at each time delay consists

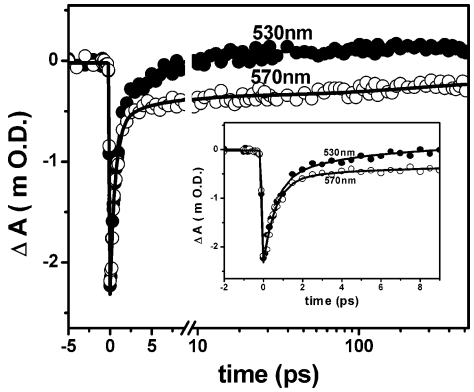

Figure 6. Bleach recovery kinetics (a) at 530 nm and (b) 570 nm in Qz/ZrO_2 system exciting with 400 nm laser light. The inset shows the same kinetics in a shorter time scale.

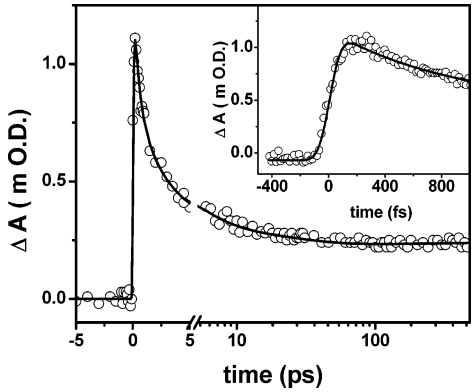

Figure 7. Decay kinetics of the injected electron at 900 nm in Qz/ZrO_2 system exciting with 400 nm laser pulse. The solid lines are best fits to the data. Displayed in the inset is the same kinetics in a shorter time scale, demonstrating electron injection time (<50 fs).

of a bleach in the 475−585 nm wavelength region centered around 510 nm, a positive peak at ∼660 nm, and a broad positive feature in the whole spectral region (750−1000 nm). From the transient spectrum it is clearly visible that photophysics of Qz molecules on the ZrO_2 nanoparticles surface is very different from that in methanol (Figure 2). Temporal characteristics of the transients in the entire wavelength region are also dissimilar to that of free Qz in solution. The positive peak at 660 nm has been attributed to the combination of cation radical of the Qz molecule as well as the injected electron in ZrO_2 nanoparticles, and the broad absorption band in the region of 750−1000 nm has been attributed to the injected electrons in the nanoparticles. Because the excited singlet state (S_1) of the Qz molecule is well below the conduction band of ZrO_2 (Scheme 1), the photoexcited Qz molecule will be unable to inject electrons into the conduction band of the ZrO_2 nanoparticles. Thus this injection process has been attributed to the injection in the surface states of nanoparticles. The bleach peak appears due to disappearance of the ground state of the dye−ZrO_2 complex, on excitation by the laser pulse. In the present investigation we have observed that the appearance time of the above signal is <50 fs; we have attributed this to the electron injection time into the surface states of ZrO_2 nanoparticles. Electron injection in the surface states of ZrO_2 nanoparticles has also been reported by Huber et al.[30] in the alizarin/ZrO_2 system. The electron injection in ZrO_2 nanoparticles can be explained by

$$ZrO_2 + Qz \leftrightarrow [ZrO_2{-}Qz]_{Adsorb} \xrightarrow[\text{electron injection}]{h\nu} e^-_{SS}(ZrO_2) + Qz^+ \quad (7)$$

The transients produced on excitation of Qz on the ZrO_2 nanoparticles surface are very different from that in neat solvent. The lifetimes of the transients found in this system are very different from that in the neat solvent. The kinetic decay of both electron in the conduction band as well as the parent cation radial and also the recovery kinetics of the bleach can provide the recombination dynamics of the injected electrons and the parent cation. Figure 6 shows the bleach recovery kinetics at 530 and 570 nm wavelengths. It is interesting to see that at early time domain (up to ∼1 ps) the recovery kinetics monitored at both the wavelengths match very well. However, at longer time domain the transient absorption at 530 nm recovers faster as compared to that at 570 nm. This indicates that the reaction scheme for the Qz/ZrO_2 system is more complex as compared to that for the Qz/TiO_2 system. As we have observed in the Qz/methanol system, the excited singlet state of Qz has a transient absorption peak at 530 nm. So our measurements in the Qz/ZrO_2 system indicate that not all excited Qz molecules are able to inject electrons into ZrO_2 nanoparticles. It is interesting to observe that although most of the Qz molecules (>95%) are adsorbed on the ZrO_2 surface, still in all the excited dye−nanoparticle systems the interfacial electron-transfer process does not take place. Hartland and co-workers have explained the presence of reactive and nonreactive sites in a 9-anthracenecarboxylate-sensitized TiO_2 system.[8] Similarly, in the present investigation, Qz molecules might have different sites of adsorption on the nanoparticle surface, reactive and nonreactive. Qz molecules, which are adsorbed at nonreactive sites cannot inject electrons into the nanoparticle. At 530 nm, on top of the bleach, the contribution due to the excited singlet absorption of Qz molecules, which do not inject electrons into the nanoparticles, is present. On the other hand, at 570 nm, the excited singlet state has negligible absorption (Figure 2). So the bleach recovery kinetics at 570 nm can give a better picture of BET dynamics in the Qz/ZrO_2 system. The recovery kinetics has been found to follow a multiexponential function with the time constants of 0.6 ps (76.2%), 4.5 ps (10.8%), and >200 ps (13%) (Table 1). Recombination dynamics of the above reaction can also be determined by both monitoring the cation radical at 660 nm and also the electron in the conduction band at 900 nm. We have also measured the electron injection time in the nanoparticles by monitoring the appearance signal of $Qz^{\bullet+}$ at 650 nm as well as e_{CB}^- at 900 nm and found to be <50 fs (inset, Figure 7). Figure 7 shows the kinetic decay trace of the conduction band electron at 900 nm. The decay trace can be fitted multiexponentially with time constants of 0.6 ps (45.6%), 4.5 ps (35.5%), and >200 ps (18.9%). We have also monitored the cation radical at 650 nm, the kinetic decay trace of the cation could be fitted multiexponentially with similar time constants as that of the electron at 900 nm. However, we believe that some fraction of Qz molecules, which are just adsorbed on the ZrO_2 nanoparticles surface and do not inject electrons, will contribute to some negative absorption at 650 nm due to stimulated emission and also for positive absorption at 900 nm due to the excited-state absorption of Qz. In other words, to measure BET dynamics in the Qz/ZrO_2 system neither 650 nor 900 nm are good wavelengths to monitor. On the other hand, at 570 nm, contributions due to the stimulated emission and excited absorption are negligible. So the bleach recovery kinetics at 570 nm is a good wavelength to determine BET kinetics. It is interesting to see that the kinetics at 570 nm has a slow component, which recombines in much longer time scale and can be assigned to the slow recombination reaction of the long-

lived charge-separated state, which occurs in the nanosecond to microsecond time scale.[52] Slow recombination reactions are due to the electrons, which are trapped at different trap depths and different distances from the adsorbate, resulting in multiexponential dynamics with many slower components.

It is interesting to observe that the transient absorption spectra of Qz-sensitized TiO_2 (Figure 3) and ZrO_2 (Figure 5) are different although in both cases the photoexcited dye Qz molecule injects electrons into the nanoparticles. This difference in spectral characteristics in Figures 3 and 5 can be explained as follows. First, we have already explained earlier in the text that Qz forms a better complex with ZrO_2 nanoparticles compared to that with TiO_2 nanoparticles and it has been well reflected in the absorption spectrum (Figure 1). As we can observe, the optical absorption spectrum of the Qz/ZrO_2 system has higher optical density in visible region (450−600 nm) compared to that in Qz/TiO_2, where in both the cases the dye and nanoparticle concentrations are the same (Figure 1). As a result, on exciting these systems (both Qz/ZrO_2 and Qz/TiO_2) one can expect higher bleach in the Qz/ZrO_2 system as compared to that in the Qz/TiO_2 system. Second, it has been observed from transient measurements that the quantum yield of electron injection in the Qz/TiO_2 system is more (∼1.6 times) than that in the Qz/ZrO_2 system. As a result, the optical density due to the cation radical in the 450−575 nm region will be higher in the Qz/TiO_2 system as compared to that in the Qz/ZrO_2 system. Takeshita et al.[54] have reported that the absorption cross-section (extinction coefficient) of the injected electron decreases as it moves to deeper and deeper trap states in semiconductor nanoparticles. So this may be another reason for lower absorption of injected electrons in the >800 nm region in the Qz/ZrO_2 system compared to that in the Qz/TiO_2 system, where the extinction coefficient of the injected electron in ZrO_2 is lower and the injected electron is deeper in nature compared to that in TiO_2. Finally, we have already discussed that the emission quantum yield of Qz decreased drastically in the presence of TiO_2 nanoparticles. On the other hand, as the injection quantum yield is low in the Qz/ZrO_2 system, so the contribution of stimulated emission yield will be higher in the Qz/ZrO_2 system compared to that in the Qz/TiO_2 system. The resultant effect of the higher extinction coefficient of the ground-state complex, higher stimulated emission yield, and lower cation yield gives a negative absorption features in the case of the Qz/ZrO_2 system. However, the features of bleach have still been observed in the case of the Qz/TiO_2 system.

(e) Electron-Transfer Dynamics in the Surface States and Importance of Coupling of the Dye Molecules with the Nanoparticles. In the present investigation we are reporting the interfacial electron-transfer dynamics of Qz-sensitized TiO_2 and ZrO_2 nanoparticles, where photoexcited Qz molecules inject electrons in the conduction of TiO_2 and surface states of ZrO_2 nanoparticles. As we have already discussed, ZrO_2 nanoparticles are used as background (noninjecting surface) to study the photophysics of excited dye molecules. However, photoexcited Qz molecules see ZrO_2 nanoparticles as an injecting surface. Electron injection into the surface states of ZrO_2 nanoparticles from photoexcited alizarin molecules has already been reported by Huber et al.[30] Not many other reports are available in the literature where injection is possible in the surface states of nanoparticles. According to Huber et al.,[30] alizarin molecules bind very strongly with both TiO_2 and ZrO_2 nanoparticles through the anthraquinone moiety. In the present investigation we have also observed a similar type of binding for Qz molecules with the nanoparticles (Chart 1). We have already described that Qz forms a strong complex with ZrO_2 nanoparticles than with TiO_2 nanoparticles (section a). We have observed from time-resolved absorption studies that the electron injection time for both TiO_2 and ZrO_2 nanoparticles is <50 fs, although the density of acceptor states in the surface sates of ZrO_2 nanoparticles is much smaller compared to that in the conduction band of TiO_2 nanoparticles. Formation of a strong CT complex with ZrO_2 nanoparticles facilitates electron injection in the surface states. The CT mechanism of injection can be explained in the following way, as already reported by Rego et al.[55] and Wang et al.[56] As the LUMO in the case of a CT complex is located on the metal center (Ti or Zr), on excitation the electron becomes directly localized on the metal center from where diffusion into either the continuum of conduction band states or the surface states of the nanoparticle takes place depending on the semiconductor. However, we have shown in Scheme 1 that electron injection in both Qz/TiO_2 and Qz/ZrO_2 systems can be possible both via photoexcited Qz molecules (k_{inj}) and also direct injection (k'_{inj}) to metal centers (Ti or Zr).

Coming to the recombination of the charge-separated species, the recombination reaction in the Qz/TiO_2 system is very fast as compared to most of the dye-sensitized TiO_2 nanoparticles reaction reported earlier, except the work reported by Huber et al.[30,57] and by us[40] in the alizarin/TiO_2 nanoparticles system and by Wang et al.[56] in the catechol/TiO_2 nanoparticles system. Huber et al.[30] reported multiexponential recombination dynamics in the alz/TiO_2 system, where the majority of the injected electron recombines very fast (430 fs). In our earlier studies[5] we have observed that strong coupling in the ground state of dye−nanoparticle systems can assist fast BET. Likely, in the Qz/TiO_2 system also we have observed fast recombination (750 fs (∼60%)) of injected electrons to the parent cation. It is very interesting to observe that in the Qz/ZrO_2 system also the majority of the injected electrons recombines with time constant ∼600 fs (76%). Recombination dynamics of the alizarin/ZrO_2 system observed by Huber et al.[30] was a little more complex than what we have observed in Qz/ZrO_2 system. The complicated decay profiles at different wavelengths reveal that in the alizarin/ZrO_2 system, immediately after the electron injection in the surface states, the injected electrons return back to the excited singlet state with time constant 450 fs. However, from the decay and recovery kinetics at different wavelengths in the Qz/ZrO_2 system (Figures 6 and 7), we have not observed any repopulation of excited singlet states in the Qz/ZrO_2 system. Repopulation of excited singlet state in the Qz/ZrO_2 system would have shown more complicated dynamics such as growth kinetics at those wavelengths (830 nm, 530 nm) where the excited singlet state of Qz molecule absorbs. However, we have not observed much complicated kinetics at any of these wavelengths. However, the presence of an excited singlet state (small contribution) at 530 nm, which is not injecting, complicated the long-time recovery but it had not complicated the fast component. So, from our experimental data we can discard any repopulation of the excited singlet state of Qz in the Qz/ZrO_2 system. In the present investigation we observed that BET kinetics in both the Qz/TiO_2 and Qz/ZrO_2 system can be fitted multiexponentially and in both cases the majority of the injected electrons recombine very fast (750 and 600 fs). What we have observed from our present studies is strength of the coupling of the dye molecule with both the nanoparticles governs the interfacial ET dynamics, both injection and BET. We have carried out transient absorption measurements studies for both Qz/TiO_2 and Qz/ZrO_2 systems by changing the excitation energy and we have not observed any changes in the charge recom-

bination dynamics. This excitation energy independence of the charge recombination tells us that the recombination is a geminate one. Similar excitation energy independence of charge recombination dynamics has been observed in the case of $Fe(CN)_6^{4-}$-sensitized TiO_2 nanoparticles by Lian and co-workers.[22]

We did not observe repopulation of the excited state in the Qz/ZrO_2 system, but Huber et al.[30] could observe repopulation in Alz/ZrO_2, which may be due to differences in the electronic structure of Alz and Qz molecules and their electronic coupling with the nanoparticles. The LUMO of alizarin (-1.5 eV[58]) is higher in energy than that of quinizarin (-0.68 eV, Scheme 1) As a result, photoexcited Alz will inject electron in the surface states of ZrO_2 nanoparticles with much higher energy as compared that of phtoexcited Qz. In such a situation in the Qz/ZrO_2 system BET may be preferred over the repopulation of the excited state.

Recently, Rego et al.[55] have studied the interfacial ET dynamics in catechol/TiO_2 nanoclusters after combining ab initio DFT molecular dynamics simulations and quantum dynamics calculations. They have found that the primary process localizes the charge in the Ti^{4+} surface ions next to the catechol adsorbate. The primary event is followed by charge delocalization (i.e., charge diffusion) through the nanocrystalline material. Ultrafast BET reaction in catechol-sensitized TiO_2 nanoparticles has been reported by Wang et al.[56] Catechols form a strong CT complex with TiO_2 nanoparticles. They have reported that the majority of the injected electrons recombine with the parent cation with time constant ~400 fs. Optical excitation of the TiO_2-cat complex promotes an electron to one or a few Ti(IV) centers near the adsorbates. BET from these centers would be very fast as compared to BET in the photoexcited molecular complex of $[NH_4]_2[Ti(cat)_3]$, as reported by Wang et al.[56] In the same way as earlier studies, the observed 600 and 750 fs components (i, Scheme 1) of BET in the present investigation for the cases of Qz/ZrO_2 and Qz/TiO_2 respectively can be explained as that of recombination of the electrons that are directly injected in the metal centers (Ti or Zr). This process of localized electron at the metal center is only possible when the dye molecules form a strong CT complex with the nanoparticles. However, the injected electrons can also rapidly delocalize and diffuse out and become trapped in different trapping positions with a distribution of trap energy and distance from the adsorbate. As a result, multiexponential recombination dynamics with time components from pico- to microsecond has been observed in both Qz/TiO_2 and Qz/ZrO_2 systems (ii, Scheme 1).

(f) Relevance to Photoelectrochemical Solar Cells. It is not possible to make a direct correlation between the results presented here and the studies of the electrical performance of dye-sensitized TiO_2 photoelectrochemical solar cells. However, it is very important to understand the basic parameters of the ET reaction in a solar cell where the dye molecules coupled strongly with the nanoparticles. In the present investigation, we have observed that Qz molecules couple strongly with the nanoparticles, forming a CT complex. For a CT complex, in principle, the electron injection efficiency should be 100%. However, the solar cell designed by Tennakone et al.[43] using organic triphenylmethane (strongly coupled with nanoparticles) dyes were found to give low photocurrent conversion efficiency (<1%). On excitation of a complex, an electron gets injected directly to the conduction band and at the same time recombination reactions are also very fast, as observed by us.[5] Solar conversion efficiency comes down due to fast BET in these CT systems.[43] Recently, Durrant and co-workers have discussed in their recent work[59,60] that device efficiency is critically dependent upon retardation of interfacial charge recombination losses and less dependent upon the interfacial injection dynamics. In the present investigation we have observed electron injection is also possible in the surface states of ZrO_2, if the dye molecules couple strongly with the nanoparticles. Here, we also get an idea of coupling matrix elements for BET of purely trap states of ZrO_2 nanoparticles. From the present studies we can conclude that a strongly coupled dye not only injects electron in the conduction band but also into the surface states of the nanoparticles. As the charge recombination reaction is very fast in these strongly coupled dye−nanoparticle systems, solar conversion efficiency will be minimizing.

4. Conclusion

Femtosecond transient absorption spectroscopy detecting in the visible and near-IR region has been used to study the electron injection and back-electron-transfer dynamics of quinizarin adsorbed onto TiO_2 and ZrO_2 nanoparticles. Steady-state absorption studies have shown that the quinone moiety of the Qz molecule forms a charge-transfer complex with ZrO_2 nanoparticles. The electron injection into the TiO_2 and ZrO_2 nanoparticles has been confirmed by monitoring the cation radical spectra at ~650 nm and the injected electron in the nanoparticles in 750−1000 nm region in real time by transient absorption spectroscopy. As the conduction band edge of ZrO_2 lies far above the S_1 state of quinizarin, the electron injection into the conduction band is not possible. The observation of the cation radical spectra in the case of the Qz/ZrO_2 system confirmed that electron injection takes place in ZrO_2 nanoparticles. We have attributed this to the injection into surface states of ZrO_2 nanoparticles. It has been observed that electron injection in both the nanoparticles takes place in <50 fs and the majority of the injected electrons come back to the parent cation with a time constant of ~500 fs for both the systems. We have observed that recombination kinetics in both the systems can be fitted multiexponentially. Ultrafast recombination dynamics of injected electrons and parent cation radicals indicate a strong coupling matrix for the BET process of the above systems. In the present investigation we have observed that strong CT complex formation facilitates electron injection in the surface states of ZrO_2 nanoparticles.

Acknowledgment. We thank Dr. G. Venkateswaran of Applied Chemistry Division, BARC, Mumbai, for his assistance in cyclic voltammetric measurements. We also thank Dr. T. Mukherjee and Dr. J. P. Mittal for their constant encouragement.

Supporting Information Available: Transient absorption spectrum of quinizarin cation radical as obtained from pulse radiolysis in N_2 saturated CCl_4 solution. This material is available free of charge via the Internet at http://pubs.acs.org.

References and Notes

(1) Oregan, B.; Gratzel, M. *Nature* **1991**, *353*, 737.
(2) Hagfeldt, A.; Gratzel, M. *Chem. Rev.* **1995**, *95*, 49.
(3) Ghosh, H. N. *J. Phys. Chem. B* **1999**, *103*, 10382.
(4) Ramakrishna, G.; Ghosh, H. N. *J. Phys. Chem. B* **2001**, *105*, 7000.
(5) Ramakrishna, G.; Ghosh, H. N. Singh, A. K.; Palit, D. K.; Mittal, J. P. *J. Phys. Chem. B* **2001**, *105*, 12786.
(6) Ramakrishna, G.; Ghosh, H. N. *J. Phys. Chem. A* **2002**, *106*, 2545.
(7) Ramakrishna, G.; Das, A.; Ghosh, H. N. *Langmuir* **2004**, *20*, 1430.
(8) Martini, I.; Hodak, J. H.; Hartland, G. V.; Kamat, P. V. *J. Chem. Phys.* **1997**, *107*, 8064.
(9) Martini, I.; Hodak, J. H.; Hartland, G. V. *J. Phys. Chem. B* **1998**, *102*, 9508.
(10) Hilgendroff, M.; Sundstrom, V. *J. Phys. Chem. B* **1998**, *102*, 10505.

(11) Benko, G.; Kallionen, J.; Korppi-Tommola, J. E. I.; Yartsev, A. P.; Sundstrom, V. *J. Am. Chem. Soc.* **2001**, *124*, 489.
(12) Moser, J.; Graetzel, M. *J. Am. Chem. Soc.* **1984**, *106*, 6557.
(13) Kamat, P. V.; Fox, M. A. *Chem. Phys. Lett.* **1983**, *102*, 379.
(14) Moser, J. E.; Gratzel, M.; Sharma, D. K.; Serpone, N. *Helv. Chim. Acta* **1985**, *68*, 1686.
(15) Eichberger, R.; Willig, F. *Chem. Phys*. **1990**, *141*, 159.
(16) Lanzafame, J. M.; Miller, R. D. J.; Muenter, A. A.; Parkinson, B. A. *J. Phys. Chem.* **1992**, *96*, 2820.
(17) Heimer, T. A.; Heilweil, E. J. *J. Phys. Chem. B* **1997**, *101*, 10990.
(18) Lu, H.; Prieskorn, J. N.; Hupp, J. T. *J. Am. Chem. Soc.* **1993**, *115*, 4927.
(19) Dang, X.; Hupp, J. T. *J. Am. Chem. Soc.* **1999**, *121*, 8399.
(20) Kuciauskas, D.; Freund, M. S.; Gray, H. B.; Winkler, J. R.; Lewis, N. S. *J. Phys. Chem. B* **2001**, *105*, 392.
(21) Argazzi, R.; Bignozzi, C. A.; Heimer, T. A.; Castellano, F. N.; Meyer, G. J. *J. Am. Chem. Soc.* **1995**, *117*, 11816.
(22) Weng, Y.; Wang, Y.; Asbury, J. B.; Ghosh, H. N.; Lian, T. *J. Phys. Chem. B* **2000**, *104*, 93−104.
(23) Ghosh, H. N.; Asbury, J. B.; Lian, T. *J. Phys. Chem. B* **1998**, *102*, 6482.
(24) Ghosh, H. N.; Asbury, J. B.; Lian, T. *Proc. Indian Natl. Sci. Acad. (PINSA)* **2000**, *66, A* (No. 2), 177−197.
(25) Ghosh, H. N.; Asbury, J. B.; Weng, Y.; Lian, T. *J. Phys. Chem. B* **1998**, *102*, 10208.
(26) Ellingson, R. J.; Asbury, J. B.; Ferrere, S.; Ghosh, H. N.; Lian, T.; Nozik, A. *J. Phys. Chem. B* **1998**, *102*, 6455.
(27) Asbury, J. B.; Ellingson, R. J.; Ghosh, H. N.; Ferrere, S.; Nozik, A.; Lian, T. *J. Phys. Chem.* **1999**, *103*, 3110.
(28) Asbury, J. B.; Hao, E.; Wang, Y. Q.; Ghosh, H. N.; Lian, T. *J. Phys. Chem. B* **2001**, *105*, 4545 (Feature Article).
(29) Haque, S. A.; Tachibana, Y.; Klug, D. R.; Durrant, J. R. *J. Phys. Chem. B* **1998**, *102*, 1745.
(30) Huber, R.; Sporlein, S.; Moser, J. E.; Gratzel, M.; Wachtveitl, J. *J. Phys. Chem B* **2000**, *104*, 8995.
(31) Nelson, J.; Haque, S. A.; Klug, D. R.; Durrant, J. R. *Phys. Rev. B* **2001**, *63*, 205321.
(32) Barzykin, A. V. Tachiya, M. *J. Phys. Chem. B* **2002**, *106*, 4356.
(33) Olsen, C. M.; Waterland, M. R.; Kelley, D. F. *J. Phys. Chem B* **2002**, *106*, 6211.
(34) Hao, E.; Anderson, N. A.; Asbury, J. B.; Lian, T. *J. Phys. Chem. B* **2002**, *106*, 10191.
(35) Bahnemann, D.; Henglein, A.; Lilie, J.; Spanhel, L. *J. Phys. Chem.* **1984**, *88*, 709.
(36) Ghosh, H. N.; Adhikari, S. *Langmuir* **2001,** *17*, 4129.
(37) Ramakrishna, G.; Ghosh, H. N. *Langmuir* **2003**, *19*, 505.
(38) Rajh, T.; Chen, L. X.; Lukas, K.; Liu, T.; Thurnauer, M. C.; Teide, D. M. *J. Phys. Chem. B* **2002**, *106*, 10543.
(39) Ramakrishna, G.; Ghosh, H. N. Unpublished Data, 2004.
(40) Ramakrishna, G.; Singh, A. K.; Palit, D. K.; Ghosh, H. N. *J. Phys. Chem. B* **2004**, *108*, 1701.
(41) Pal, H.; Palit, D. K.; Mukherjee, T.; Mittal, J. P. *J. Chem. Soc., Faraday Trans.* **1991**, *87* (8), 1109.
(42) Cherepy, N. J.; Smestad, G. P.; Gratzel, M.; Zhang, J. Z. *J. Phys. Chem. B* **1997**, *101*, 9342.
(43) Jayaweera, P. M.; Kumarasinghe, A. R.; Tennakone, K. *J. Photochem. Photobiol. A: Chem.* **1999**, *126*, 111.
(44) Yarwood, J. *Spectroscopy and Structure of Molecular Complexes*; Plenum Press: New York, 1970.
(45) Chen, L. X.; Rajh, T.; Wang M. C.; Thurnauer, M. C. *J. Phys. Chem. B* **1998**, *101*, 10688.
(46) Marcus, R. A.; Sutin, N. *Biochim. Biophys. Acta* **1985,** *811*, 265.
(47) Mulliken, R. S. *J. Am. Chem. Soc.* **1952**, *64*, 811. Mulliken, R. S.; Person, W. B. *Molecular Complexes*; Wiley: NewYork, 1969.
(48) Hush, N. S. *Prog. Inorg. Chem.* **1967**, *8*, 391; *Electrochim. Acta* **1968**, *13*, 1005.
(49) Zhang, J. Z. *Acc. Chem. Res.* **1997,** *30*, 423.
(50) Colombo, D. P., Jr.; Bowman, R. M. *J. Phys. Chem.* **1996**, *100*, 18445.
(51) Skimmer, D. E.; Colombo, D. P. Jr.; Cavaleri, J. J.; Bowman, R. M. *J. Phys. Chem.* **1995**, *99*, 7853.
(52) See Supporting Information. Also see: Ramakrishna, G.; Ghosh, H. N. Unpublished work, 2004.
(53) Kay, A.; Humphry-Baker, R.; Gratzel, M. *J. Phys. Chem.* **1994**, *98*, 952.
(54) Takeshita, K.; Sasaki, Y.; Kobashi, M.; Tanaka, Y.; Maeda, S.; Yamakata, A.; Ishibashi, T.; Onishi, H. *J. Phys. Chem. B* **2003,** *107*, 4156.
(55) Rego, G. L. S., Batista, V. S. *J. Am. Chem. Soc.* **2003**, *125*, 7989
(56) Wang, Y.; Hang, K.; Anderson, N. A.; Lian, T. *J. Phys. Chem. B* **2003**, *107*, 9434.
(57) Huber, R.; Moser, J. E.; Gratzel, M.; Wachtveitl, J. *J. Phys. Chem B* **2002**, *106*, 6494.
(58) Shoute, L. C. T.; Loppnow, G. R. *J. Chem. Phys.* **2002**, *117*, 842.
(59) Palomares, E.; Clifford, J. N.; Haque, S. A.; Lutz, T.; Durrant, J. R. *J. Am. Chem. Soc.* **2003**, *125*, 475.
(60) Tachibana, Y.; Nazeeruddin, M. K.; Gratzel, M.; Klug, D. R.; Durrant, J. R. *Chem. Phys.* **2002**, *285*, 127.